Clim Dyn (2014) 43:2399–2414
DOI 10.1007/s00382-014-2062-3

Effectiveness of the Bjerknes stability index in representing ocean dynamics

Felicity S. Graham · Jaclyn N. Brown · Clothilde Langlais · Simon J. Marsland · Andrew T. Wittenberg · Neil J. Holbrook

Received: 5 September 2013 / Accepted: 21 January 2014 / Published online: 12 February 2014

Abstract The El Niño-Southern Oscillation (ENSO) is a naturally occurring coupled phenomenon originating in the tropical Pacific Ocean that relies on ocean–atmosphere feedbacks. The Bjerknes stability index (BJ index), derived from the mixed-layer heat budget, aims to quantify the ENSO feedback process in order to explore the linear stability properties of ENSO. More recently, the BJ index has been used for model intercomparisons, particularly for the CMIP3 and CMIP5 models. This study investigates the effectiveness of the BJ index in representing the key ENSO ocean feedbacks—namely the thermocline, zonal advective, and Ekman feedbacks—by evaluating the amplitudes and phases of the BJ index terms against the corresponding heat budget terms from which they were derived. The output from Australian Community Climate and Earth System Simulator Ocean Model (a global ocean/sea ice flux-forced model) is used to calculate the heat budget in the equatorial Pacific. Through the model evaluation process, the robustness of the BJ index terms are tested. We find that the BJ index overestimates the relative importance of the thermocline feedback to the zonal advective feedback when compared with the corresponding terms from the heat budget equation. The assumption of linearity between variables in the BJ index formulation is the primary reason for these differences. Our results imply that a model intercomparison relying on the BJ index to explain ENSO behavior is not necessarily an accurate quantification of dynamical differences between models that are inherently nonlinear. For these reasons, the BJ index may not fully explain underpinning changes in ENSO under global warming scenarios.

Keywords ENSO dynamics · Bjerknes stability index

Electronic supplementary material The online version of this article (doi:10.1007/s00382-014-2062-3) contains supplementary material, which is available to authorized users.

F. S. Graham (✉) · N. J. Holbrook
Institute for Marine and Antarctic Studies, University of Tasmania, GPO Box 1538, Hobart, Tasmania 7001, Australia
e-mail: fsm@utas.edu.au

J. N. Brown · C. Langlais
Wealth from Oceans National Research Flagship, CSIRO Marine and Atmospheric Research, Hobart, Australia

S. J. Marsland
CSIRO Marine and Atmospheric Research, Aspendale, Australia

A. T. Wittenberg
National Oceanographic and Atmospheric Administration, Geophysical Fluid Dynamics Laboratory, Princeton, USA

N. J. Holbrook
ARC Centre of Excellence for Climate System Science, Institute for Marine and Antarctic Studies, University of Tasmania, Hobart, Australia

1 Introduction

Since Bjerknes (1969) first introduced the notion that El Niño-Southern Oscillation (ENSO) resulted from coupled ocean–atmosphere interactions in the equatorial Pacific, great advances have been made in understanding the dynamics of this phenomenon (Wyrtki 1975; Cane and Zebiak 1985; Zebiak and Cane 1987; Battisti 1988; Schopf and Suarez 1988; Battisti and Hirst 1989; Philander 1990; Picaut et al. 1996; Jin 1997a). Nonetheless, there are a diverse range of ENSO behaviors both within and between coupled general circulation models (CGCMs), including differences in the frequency and amplitude of the coupled ENSO mode, in the asymmetry of ENSO events, and in the

behavior and type of dynamics that play a role (Wittenberg 2009; Vecchi and Wittenberg 2010; Collins et al. 2010; Watanabe et al. 2012; Choi et al. 2013).

Previous studies have argued that diversity between CGCMs can be attributed to variations in the modeled background ocean–atmosphere state of the equatorial Pacific, which alter the coupled instability (Philander et al. 1984; Neelin and Jin 1993; Fedorov and Philander 2001). In keeping with this theory, Jin et al. (2006) derived a coupled ENSO stability index, called the Bjerknes stability index (BJ index), from the mixed layer heat budget equation with the aim of (1) depicting the growth rate of the leading coupled ENSO-like mode, and (2) understanding and quantifying ENSO diversity in CGCMs based on a variety of mean states. The BJ index is given by the constant R, which represents the Bjerknes positive feedback. This index quantifies the key processes involved in equatorial Pacific ocean–atmosphere dynamics—namely advection by mean currents, thermodynamic damping, the thermocline feedback, the zonal advective feedback, and the Ekman feedback. The metric R is derived from the coupled system of equations that collectively describe the recharge oscillator model (Jin 1997a, b), that is

$$\left\langle \frac{\partial T}{\partial t} \right\rangle_E = R\langle T \rangle_E + F\langle h \rangle_W, \tag{1}$$

$$\left\langle \frac{\partial h}{\partial t} \right\rangle_E = -\epsilon\langle h \rangle_W - \tilde{F}[\tau^x], \tag{2}$$

where $\langle T \rangle_E$ is the volume averaged temperature from the sea surface to the depth of the mixed layer in the central-eastern equatorial Pacific 5°S–5°N, 175°E–80°W, $\langle h \rangle_W$ is the thermocline depth averaged in the western equatorial Pacific (5°S–5°N, 120–175°E), and $[\tau^x]$ is the zonal wind stress anomaly averaged across the entire equatorial Pacific basin (5°S–5°N, 120°E–80°W) and is related to $\langle T \rangle_E$ by $[\tau^x] = \lambda\langle T \rangle_E$, where λ can be estimated via regression analysis. F and $\tilde{F}$ are constants representing the frequency of the interannual oscillation of the system and Sverdrup transport across the equatorial Pacific basin, respectively. Finally, ϵ is the damping rate of ocean adjustment. Angle brackets denote volume averaged quantities and square brackets denote variables that have been averaged across the full equatorial Pacific basin.

The BJ index has many useful applications and has aided understanding of the dynamics of the climate system. The BJ index is in good agreement with the linear growth rates of intermediate-complexity models and more complex CGCMs under changing background states, demonstrating its potential usefulness in evaluating the stability of coupled models (Jin et al. 2006; Kim and Jin 2010a). Lübbecke and McPhaden (2013) used the BJ index to compare coupled instabilities in the Pacific and Atlantic ENSO-like modes, which allowed them to demonstrate that the Atlantic was overall more damped than the Pacific, most likely due to a weaker thermocline feedback. The BJ index has also been used in model intercomparison studies to assess changes in ENSO stability under historical and future climatic conditions. Kim and Jin (2010b) compared the BJ index estimated from 12 CGCMs among the Coupled Model Intercomparison Project phase 3 (CMIP3) in both historical and increased CO_2 climates, finding that the positive ocean feedbacks were likely to grow under global warming. However, the CGCMs were diverse in their representation of ENSO characteristics, which limited the reliability of this conclusion. More recently, Kim et al. (2013) applied the BJ index to a suite of CMIP5 models and compared the estimated growth rates with observations. They argue that, due to the cold tongue bias, the majority of CMIP5 models underestimate the magnitude of the positive ocean feedback terms compared with observations.

It is well known that CGCMs suffer biases in the tropical Pacific, such as the cold tongue bias, and biases in the seasonal cycle and the western Pacific warm pool edge, that affect the frequency, amplitude, and dynamics of the simulated ENSO (Guilyardi et al. 2009; Sen Gupta et al. 2012). While the BJ index attempts to account for such diversity between CGCMs through quantification of the mean state, by the use of averaging regions that are fixed in space the BJ index is limited in the extent to which it can account for the diversity in location and spread of ENSO events, both within and across CGCMs. A further difficulty with using the BJ index to compare CGCMs is in choosing an appropriate time period over which to calculate the BJ index. That is, internal variability within models leads to a range of spatial "flavors" of ENSO in which local and remote ENSO dynamics dominate to varying degrees (Ashok et al. 2007; Kug et al. 2010; Karnauskas 2013). Comparing CGCMs over time periods characterized by different spatial "flavors" of ENSO may lead to conflicting results from the BJ index, even when the underlying dynamics are not necessarily markedly different. This is a particularly important consideration when applying the BJ index to CGCM simulations of future climate scenarios.

Studies applying the BJ index to observations or reanalysis products have found that the thermocline feedback is at least twice the magnitude of the zonal advective feedback (Lübbecke and McPhaden 2013; Kim et al. 2013). This result conflicts with that of Jin and An (1999), who used a simple model to compare the roles of the thermocline and zonal advective feedbacks in the Niño-3 region (5°S–5°N, 150–90°W) and found that the two feedbacks made similar contributions to changes in the temperature tendency. Results from mixed layer heat budget analyses of the National Center for Environmental

Prediction coupled model support the finding that the zonal advective feedback and the thermocline feedback are of a similar magnitude (Huang et al. 2010, 2011). However, Dewitte et al. (2013) highlight the difficulty in determining the importance of the thermocline feedback over the zonal advective feedback, due to changes in the relative strength of each feedback over time. In particular, since 1976 the thermocline feedback has become more effective at influencing the sea surface temperature (SST) in the Niño-4 region (5°S–5°N, 160°E–150°W) than the zonal advective feedback due to an increase in vertical stratification. Nevertheless, causes for the overestimation of the thermocline feedback with respect to the zonal advective feedback in the BJ index have not been identified.

The BJ index describes the climate system using linear equations. However, studies of atmospheric forcing in the equatorial Pacific have demonstrated that a phase nonlinearity exists in the observed and modeled relationship between the shortwave component of the heat flux and the SST (Lloyd et al. 2012; Bellenger et al. 2013). As a result, the assumption of linearity in the calculation of the BJ index thermodynamic damping coefficient may mask the extent of this nonlinearity. Whether the assumption of linearity in the ocean components of the BJ index is robust is yet to be established.

Given that the BJ index has been used to understand climate dynamics, climate change, and to assess model performance, we examine whether the formulation of the BJ index is effective in capturing the key ocean dynamics important to ENSO. Using a global ocean/sea ice model simulation of the period 1980–2007, we contrast the magnitudes and phases of the feedback terms calculated from the model using the BJ index with the corresponding heat budget feedbacks that the BJ index approximates. As the BJ index terms are derived as simplifications of the heat budget terms, we explore how well they still capture the underlying ocean dynamics. The robustness of the assumption of linearity in the individual balance equations used to derive the ocean feedbacks is analyzed. Where the assumption of linearity is inappropriate, we consider the implications on the reliability and accuracy of the BJ index. We demonstrate that the BJ index may not accurately quantify the underlying ocean dynamics of the model, which has implications for studies that rely on the BJ index to measure model performance, to perform model intercomparisons, and to assess how global warming affects ENSO dynamics.

Section 2 describes the climate model run used in this study, the method used to calculate the mixed layer heat budget in the equatorial Pacific, and the BJ index calculation. In Sect. 3, the positive ocean feedbacks from the BJ index are compared with the respective terms from the heat budget. Sections 4 and 5 provide a discussion and summary of the results.

2 Data and methods

In this study, the output from a global ocean/sea ice model simulation was analyzed. We choose to analyze the output from a flux-forced ocean/sea ice model rather than from a coupled ocean/atmosphere/sea ice model so that our calculations of the mixed layer heat budget and BJ index are not confounded by the errors that arise in the latter due to model biases. Furthermore, using an ocean/sea ice model is advantageous as the SST (mean state and variability) from flux-forced ocean/sea ice models is constrained to agree with observational products from which many of the underlying assumptions of the BJ index are derived. An alternative would be to use reanalysis data; however, this may introduce further complications in that the data is not dynamically consistent (Oke et al. 2013). Further, the goal of this study is to provide an example of how the BJ index can be misleading when studying model intercomparisons of ENSO dynamics, not to accurately evaluate the BJ index terms. To this end, the use of ocean model data is most appropriate and adequate for our demonstration purposes. In the following section, the mixed-layer heat budget is defined and calculated, and the BJ index is introduced.

2.1 ACCESS-OM

Monthly means from the Australian Community Climate and Earth System Simulator Ocean Model (ACCESS-OM; Bi et al. 2013), that couples the NOAA/GFDL ocean model MOM4p1 (Griffies 2009) and the LANL sea ice model CICE4.1 (Hunke and Lipscomb 2010), are calculated and analyzed. In general, ACCESS-OM has a horizontal resolution of 1° with the following three refinements: a tripolar grid (Murray 1996) north of 65°N; a cosine dependent meridional grid spacing in the Southern Ocean; and a meridional resolution of 1/3° between 10°S and 10°N, gradually extending to 1° between 10°S (°N) and 20°S (°N). The vertical discretization uses a z^* coordinate (Adcroft and Campin 2004) and there are 50 vertical levels with a resolution extending from 10m in the upper 200m to approximately 333m in the deep ocean. The model run is forced with surface heat, freshwater, and momentum fluxes derived from the forcing and bulk-formulae of Large and Yeager (2009). The simulation uses the protocols of the CLIVAR Working Group on Ocean Model Development Coordinated Ocean-Ice Reference Experiments version 2 (CORE-v2) as described in Griffies et al. (2012) and first utilized in Danabasoglu et al. (2014).

The mixing scheme in ACCESS-OM combines three different parameterizations: (1) the K profile parameterization (KPP) for the surface mixed layer (Large et al. 1994); (2) a tidal mixing parameterization for the abyssal ocean (Simmons et al. 2004) and coastal oceans (Lee et al. 2006); and (3) a constant background diffusivity of 1.0×10^{-5} m^2 s^{-2} elsewhere. A linear sea surface salinity (SSS) restoring with a timescale of 60 days is used in the upper model layer. Water mass fluxes instead of virtual salt fluxes are employed in the upper boundary and water volume is conserved using a global ocean water flux correction.

In general, the ACCESS-OM simulation of the tropical Pacific compares well with observations (Online Resources 1-3; Bi et al. 2013). However, the thermocline is slightly shallower than the observations in the eastern equatorial Pacific, which gives rise to zonal currents that are stronger than observed in the eastern equatorial Pacific (Online Resources 1 and 2).

We applied a low-pass filter to the data to remove variability with frequencies shorter than 90 days. This 90 day cutoff period was chosen to separate seasonal and interannual variability from phenomena with shorter timescales, such as Tropical Instability Waves (TIWs), oceanic Kelvin waves, the Madden-Julian oscillation and westerly wind bursts, consistent with other studies (e.g. Kessler et al. 1998).

2.2 Mixed layer depth definition

The mixed layer depth (MLD) was defined according to a constant density threshold; the depth at which a density difference of 0.125 kg m^{-3} compared to the surface was first reached. As demonstrated by Huang et al. (2010), this is an appropriate criterion to calculate the MLD in the equatorial region, and the results of the heat budget analysis should not be sensitive to the choice of criterion. For the ACCESS-OM model, this choice of MLD definition produced estimates of the MLD that agreed with observations from the CSIRO atlas of regional seas (CARS atlas; Ridgway et al. 2002) (figure not shown).

2.3 Mixed layer heat budget

The equation for the mixed layer heat budget can be written

$$\frac{\partial T}{\partial t} = Q_q - \mathbf{u} \cdot \nabla T - w_e \frac{T - T_H}{H_{HB}} + Res, \tag{3}$$

(e.g. Qu 2003; Santoso et al. 2010; Schiller and Ridgway 2013). Here, $\partial T/\partial t$ is the potential temperature tendency averaged in the mixed layer, Q_q is the net downward surface heat flux, which combines the shortwave, longwave, sensible, and latent heat fluxes at the surface omitting the amount of shortwave heat that penetrates through the base of the mixed layer, $\mathbf{u}$ is the two dimensional vertically-averaged horizontal velocity vector, and the term $\mathbf{u} \cdot \nabla T$ represents horizontal advection of heat. The residual term *Res* represents unresolved processes, including high frequency eddies, vertical and lateral diffusion, and any spurious numerical diffusion. The second to last term on the right hand side of Eq. (3) represents vertical advection into the mixed layer, where w_e is the vertical entrainment velocity and the term multiplied by w_e is a parameterization of the vertical temperature gradient calculated via the difference between the mixed layer temperature T and the temperature at the grid point just below the mixed layer T_H, divided by the temporally and spatially varying MLD (H_{HB}). The vertical entrainment velocity is given by

$$w_e = \frac{\partial H_{HB}}{\partial t} + \mathbf{u}_H \cdot \nabla H_{HB} + w_H, \tag{4}$$

where $\mathbf{u}_H \cdot \nabla H_{HB}$ is the horizontal velocity vector at the base of the mixed layer $\mathbf{u}_H$ multiplied by the corresponding horizontal gradient of the MLD ∇H_{HB}. The vertical velocity at the base of the mixed layer is given by w_H. Since from below only mean entrainment into the mixed layer affects the mixed layer temperature, we introduce the Heaviside step function notation, $H(\overline{w_e})$, where

$$H(x) = \begin{cases} 1, & x > 0 \\ 0, & \text{otherwise}, \end{cases}$$

to denote that the vertical entrainment velocity must be positive definite.

Equation (3) is decomposed into seasonal climatologies (denoted by an overbar) and anomalies (denoted by a prime), yielding the following mixed layer anomalous heat budget equation

$$\begin{aligned} \frac{\partial T'}{\partial t} &= Q'_q - \mathbf{u}' \cdot \nabla \overline{T} - \overline{\mathbf{u}} \cdot \nabla T' - \mathbf{u}' \cdot \nabla T' + \overline{\mathbf{u}' \cdot \nabla T'} \\ &\quad - H(\overline{w_e}) w'_e \frac{\overline{T} - \overline{T_H}}{H_{HB}} - H(\overline{w_e}) \overline{w_e} \frac{T' - T'_H}{H_{HB}} \\ &\quad - H(\overline{w_e}) w'_e \frac{T' - T'_H}{H_{HB}} + \overline{H(\overline{w_e}) w'_e \frac{T' - T'_H}{H_{HB}}} + Res', \\ &= S' + Res'. \end{aligned} \tag{5}$$

Note that we apply the Heaviside step function to the climatological vertical entrainment velocity in each case. This is for consistency with the BJ index calculation below and with Kim and Jin (2010a), and yields a better approximation to the linear relation in Eq. (15). The temperature tendency $\partial T'/\partial t$ and S' are volume averaged in the central-eastern equatorial Pacific 5°S–5°N, 175°E–80°W; Fig. 1) and denoted $\langle \partial T/\partial t \rangle_E$ and $\langle S \rangle_E$, respectively (note that

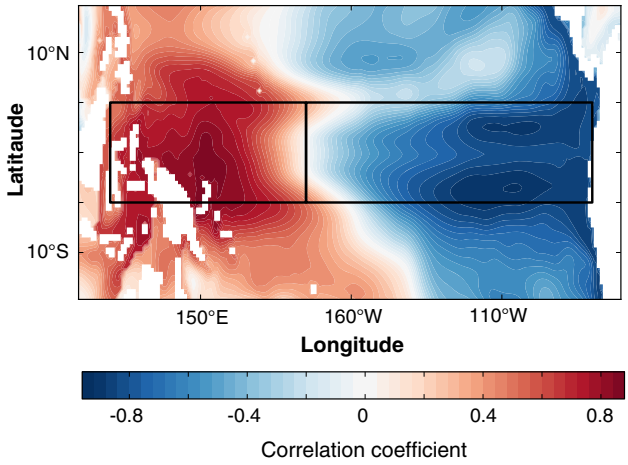

Fig. 1 The correlation field of the leading EOF mode of upper ocean heat content anomalies in the equatorial Pacific. The boxes delineate the western Pacific region from the central-eastern Pacific region for the purposes of our study

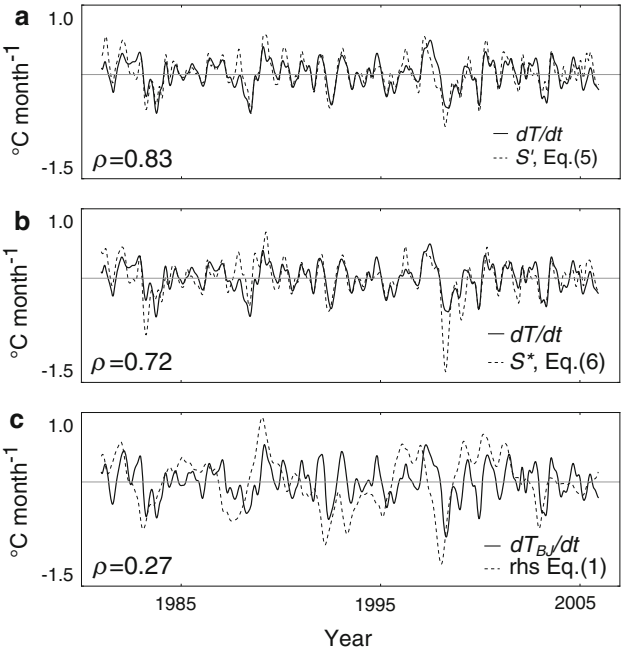

Fig. 2 Closure of the temperature tendency. **a** is the anomalous heat budget equation in Eq. (5); **b** is the anomalous heat budget equation including only the terms corresponding to those in the BJ index, that is Eq. (6); and **c** is the BJ index formulation of the recharge oscillator temperature equation, Eq. (1). In each, the *solid line* is the anomalous temperature tendency, $\langle \partial T/\partial t \rangle_E$, and the *dashed line* is the right-hand side of the corresponding equations. Note that the temperature tendency in **c** differs from the *upper panels* due to the constant rather than variable MLD in the BJ index formulation. The correlation coefficients between the two timeseries in *each panel* are reported (ρ values). A low-pass filter to remove variability of 90 days and less was applied to each of the timeseries. The mean of each timeseries in the *three panels* is close to zero

here, and in what follows, the prime notation used to denote an anomaly has been dropped). Figure 2a shows the time evolution of $\langle \partial T/\partial t \rangle_E$ and $\langle S \rangle_E$ over the period 1980–2007. The curves $\langle \partial T/\partial t \rangle_E$ and $\langle S \rangle_E$ correlate well ($\rho = 0.83$), indicating that the right-hand side of Eq. (5), even when the residual terms are omitted, is a good approximation to the mixed layer temperature tendency of the equatorial Pacific. The main discrepancies between $\langle \partial T/\partial t \rangle_E$ and $\langle S \rangle_E$ arise during large ENSO events, for instance 1982–1983 and 1997–1998, when there were notable changes to TIW behavior. It is expected that there would be better agreement between the two curves with the addition of vertical diffusion terms, which play an important role in ENSO events (e.g. Zhang and McPhaden 2010).

In the derivation of the BJ index, the nonlinear terms from the heat budget are neglected. The heat budget, now containing only the features considered by the BJ index, is

$$\left\langle \frac{\partial T}{\partial t} \right\rangle_E = \underbrace{-\left(\langle \overline{u} \rangle_E \left\langle \frac{\partial T}{\partial x} \right\rangle_E + \langle \overline{v} \rangle_E \left\langle \frac{\partial T}{\partial y} \right\rangle_E \right)}_{(1)} + \underbrace{\langle Q_q \rangle_E}_{(2)} + \underbrace{\langle H(\overline{w_e}) \overline{w_e} \rangle_E \left\langle \frac{\partial T}{\partial z} \right\rangle_E}_{(3)} - \underbrace{\langle u \rangle_E \left\langle \frac{\partial \overline{T}}{\partial x} \right\rangle_E}_{(4)} + \underbrace{\langle H(\overline{w_e}) w_e \rangle_E \left\langle \frac{\partial \overline{T}}{\partial z} \right\rangle_E}_{(5)}, = \langle S^* \rangle_E, \tag{6}$$

where $\langle \partial T/\partial z \rangle_E = \langle -(T - T_H)/H_{HB} \rangle_E$, and the terms on the right-hand side of the equation represent (1) advection due to mean zonal and meridional currents, (2) thermodynamic damping, (3) the thermocline feedback, (4) the zonal advective feedback, and (5) the Ekman feedback, respectively. Note the neglect of the spatial eddy terms in Eq. (5). As above, the angle brackets denote volume averaged variables and the subscript E denotes averaging in the central-eastern box. The two sides of Eq. (6) are plotted in Fig. 2b. The correlation coefficient between the left- and right-hand sides is 0.72.

Comparison of Fig. 2a and b illustrates the effect of removing the nonlinear terms on the closure of the heat budget. As expected, there is poorer closure during the large ENSO events of 1982–1983 and 1997–1998. There is also poor closure during the 1988−1989 La Niña event. In this case, that the preceding 1986–1987 El Niño event was not phase locked to the seasonal cycle may have given rise to nonlinearities that were not present during other events.

2.4 The BJ index

The BJ index is derived from the mixed layer heat budget equation, with the nonlinear terms omitted [Eq. (6)], and a series of linear balance relations obtained from

approximations to the ENSO ocean–atmosphere coupled dynamics (c.f. Battisti and Hirst 1989; Jin 1997a; Jin and An 1999; An and Jin 2001; Jin et al. 2006). An outline of the BJ index derivation is provided in the "Appendix". The BJ index is a constant number evaluated as R, where

$$R = \underbrace{-\left(\frac{\langle \overline{u} \rangle_E}{L_x} + \frac{\langle -2y\overline{v} \rangle_E}{L_y^2} + \frac{\langle \overline{w} \rangle_E}{H_{BJ}}\right)}_{(1)} \underbrace{-\alpha}_{(2)} + \underbrace{a_h \beta_h \mu \left\langle \frac{\overline{w}}{H_{BJ}} \right\rangle_E}_{(3)} + \underbrace{\beta_u \mu \left\langle -\frac{\partial \overline{T}}{\partial x} \right\rangle_E}_{(4)} + \underbrace{\beta_w \mu \left\langle -\frac{\partial \overline{T}}{\partial z} \right\rangle_E}_{(5)}. \tag{7}$$

The terms on the right-hand side of Eq. (7) are (1) advection by mean currents, (2) thermodynamic damping, (3) the thermocline feedback, (4) the zonal advective feedback, and (5) the Ekman feedback, and can be related to the corresponding terms in Eq. (6). The constant coefficients β_h, β_u, β_w measure the sensitivity of the response of different oceanic variables (i.e. $\langle h \rangle_E - \langle h \rangle_W$, $\langle u \rangle_E$, and $\langle w \rangle_E$) to wind stress forcing at the surface, the coefficient μ is the air–sea coupling coefficient, and the coefficient a_h measures the sensitivity of the mixed layer temperature response to changes in the thermocline depth. L_x and L_y are the longitudinal and latitudinal extents of the central-eastern box, respectively, and the factor $-2y/L_y$ assumes that the tropical SST anomalies are Gaussian with an e-folding decay scale of L_y. We note that the terms in Eq. (7) are only the components of the heat budget that contribute to growth R as described in Eq. (1). The components of the heat budget that contribute to frequency F are

$$F = \beta_{uh} \left\langle -\frac{\partial \overline{T}}{\partial x} \right\rangle_E + a_h \left\langle \frac{\overline{w}}{H_{BJ}} \right\rangle_E. \tag{8}$$

Details of how the terms in Eqs. (7) and (8) are derived from Eq. (6) are given in the "Appendix".

Consistent with previous studies (Jin et al. 2006; Kim and Jin 2010a), the BJ index is calculated by estimation of the sensitivity coefficients in Eq. (7) from linear least squares regression, where in each case the intercept is constrained to be zero. Error bounds for the 95 % confidence levels are also calculated. The spatial boxes for averaging the feedbacks in the BJ index are determined using empirical orthogonal function (EOF) analysis of upper ocean heat content anomalies (defined as the volume averaged temperature in the uppermost 300m of the equatorial ocean). Here, the upper ocean heat content is used as a proxy for thermocline depth (the depth of the 20°C isotherm), which is a good approximation in the equatorial ocean (e.g. Rebert et al. 1985), for ease of comparison with previous studies. The results of the EOF analysis for the full equatorial Pacific between 15°S–15°N and from 120°E–80°W are shown in Fig. 1. The 175°E line is identified as delineating the western box (5°S–5°N and 120–175°E) from the central-eastern box (5°S–5°N and 175°E–80°W). The temperature anomaly $\langle T \rangle_E$ and the net downward surface heat flux anomaly $\langle Q \rangle_E$ are both averaged in the central-eastern box; the upper ocean heat content anomaly is averaged in the central-eastern box $\langle h \rangle_E$ and the western box $\langle h \rangle_W$; and the zonal wind stress anomalies are averaged collectively over the western and central-eastern boxes $[\tau^x]$. In the boxed regions, $[\tau^x]$ and $\langle Q \rangle_E$ are area averaged and the remaining variables are volume averaged between the surface and a constant MLD of $H_{BJ} = 50$m. The assumption of a constant MLD in the BJ index introduces an error in the estimation of the feedback terms of a similar order to the feedbacks themselves, and is also investigated. The parameterization of $\langle \partial T/\partial z \rangle_E$ in the mixed layer heat budget definition is $\langle \partial T/\partial z \rangle_E \approx \langle -(T - T_H)/H_{HB} \rangle_E$. In the BJ index, this term is split into two components: the first component $\langle -T/H_{BJ} \rangle_E$ contributes to advection by mean currents; the second, denoted $\langle \partial T/\partial z \rangle_E \approx \langle T_H/H_{BJ} \rangle_E$, contributes to the thermocline feedback.

3 Analysis of the BJ index

The feedback terms in the BJ index are calculated and compared with the corresponding terms calculated from the mixed layer heat budget equation, Eq. (5). A more detailed derivation of the BJ index from the heat budget appears in the "Appendix".

3.1 The recharge oscillator using the BJ index

First, we address how well the recharge oscillator description of ENSO reproduces the volume averaged temperature anomaly tendency with the BJ index definition of R and F. The terms in Eq. (1), which appear in more detail in Eq. (20) from the "Appendix", were calculated and the left- and right-hand sides of this equation plotted in Fig. 2c. The BJ index formulation of the temperature tendency—the right-hand side of Eq. (1)—does a poor job of modeling the true temperature tendency in the ACCESS-OM output; the correlation coefficient between the two curves is 0.27 (Table 1). The BJ formulation of the temperature tendency appears to capture the low frequency variability of the temperature tendency. Hence, as expected, the correlation coefficient for the same two timeseries when a 12-month filter is applied is slightly higher ($\rho = 0.38$). There is poor budget closure during the periods

Table 1 Correlation coefficients (ρ) between the left- and right-hand sides of each of the equations listed

	Eq.	ρ
Full anomalous heat budget, $\left\langle \frac{\partial T}{\partial t} \right\rangle_E = \langle S \rangle_E$	(5)	0.83
Heat budget equivalent to BJ index, $\left\langle \frac{\partial T}{\partial t} \right\rangle_E = \langle S^* \rangle_E$	(6)	0.72
BJ index temperature tendency, $\left\langle \frac{\partial T}{\partial t} \right\rangle_E = R\langle T \rangle_E + F\langle h \rangle_W$	(1)	0.27
Thermocline feedback		
$-\langle H(\overline{w_e})\overline{w_e} \rangle_E \left\langle \frac{\partial T}{\partial z} \right\rangle_E = a_h \beta_h \mu \left\langle \frac{\overline{w}}{H_{BJ}} \right\rangle_E \langle T \rangle_E$		0.60
(i) $\langle H(\overline{w}) T_H \rangle_E = a_h \langle h \rangle_E$,	(9)	0.91
(ii) $\langle h \rangle_E - \langle h \rangle_W = \beta_h [\tau^x]$,	(10)	0.86
(iii) $[\tau^x] = \mu \langle T \rangle_E$,	(11)	0.84
Full thermocline feedback		
$-\langle H(\overline{w_e})\overline{w_e} \rangle_E \left\langle \frac{\partial T}{\partial z} \right\rangle_E = a_h \beta_h \mu \left\langle \frac{\overline{w}}{H_{BJ}} \right\rangle_E \langle T \rangle_E + a_h \left\langle \frac{\overline{w}}{H} \right\rangle_E \langle h \rangle_W$	(12)	0.51
Zonal advective feedback		
$-\langle u \rangle_E \left\langle \frac{\partial \overline{T}}{\partial x} \right\rangle_E = \beta_u \mu \left\langle -\frac{\partial \overline{T}}{\partial x} \right\rangle_E \langle T \rangle_E$		0.45
(i) $\langle u \rangle_E = \beta_u [\tau^x] + \beta_{uh} \langle h \rangle_W$,	(13)	0.68
Full zonal advective feedback		
$-\langle u \rangle_E \left\langle \frac{\partial \overline{T}}{\partial x} \right\rangle_E = \beta_u \mu \left\langle -\frac{\partial \overline{T}}{\partial x} \right\rangle_E \langle T \rangle_E + \beta_{uh} \left\langle -\frac{\partial \overline{T}}{\partial x} \right\rangle_E \langle h \rangle_W$	(14)	0.58
Ekman feedback		
$-\langle w_e \rangle_E \left\langle \frac{\partial \overline{T}}{\partial z} \right\rangle_E = \beta_w \mu \left\langle -\frac{\partial \overline{T}}{\partial z} \right\rangle_E \langle T \rangle_E$		0.14
(i) $\langle H(\overline{w}) w \rangle_E = -\beta_w [\tau^x]$,	(15)	0.82
Thermodynamic damping $\alpha \langle T \rangle_E$		
(i) $\langle Q \rangle_E = -\alpha \langle T \rangle_E$,	(17)	0.90

1992–1995 and 1999–2003. However, central Pacific El Niño events (i.e. events that occur near the western Pacific warm pool region), which are characterized by a less strong recharge mechanism than eastern Pacific El Niño events (Ren and Jin 2013), occurred during these two periods (Singh et al. 2011). Thus, given that the right-hand side of Eq. (1) assumes a robust recharge mechanism, it is perhaps not surprising that poorer closure is observed in 1992–1995 and 1999–2003.

We investigate whether the lack of agreement between the left- and right-hand sides of Eq. (1) is due to (a) omitting the nonlinear terms from the heat budget Eq. (5), or (b) a poor representation of the terms in the BJ index. To determine this, we compare the terms from the heat budget that correspond to the BJ index temperature tendency formulation, that is, Fig. 2b and c. If these are similar, then the error in the recharge oscillator is due to omitting the nonlinear terms from the heat budget Eq. (5); otherwise, it is due to poor approximations of the heat budget terms it does contain. The heat budget formulation more accurately captures the shape and variability of the temperature tendency and explains a higher proportion of the variance in the temperature tendency ($\rho = 0.72$; $\rho^2 = 0.52$) compared with the BJ index formulation ($\rho = 0.27$; $\rho^2 = 0.07$). Hence, we conclude that at least some of the assumptions underlying the BJ index formulation are either incorrect or inadequate in explaining ENSO dynamics, rather than there being a problem with the omission of terms. Next, we investigate the three ocean feedback terms separately to explore how and why the BJ index does not represent the ocean dynamics correctly over this period.

3.2 Thermocline feedback

The BJ index form of the thermocline feedback is given by

$$a_h \beta_h \mu \left\langle \frac{\overline{w}}{H_{BJ}} \right\rangle_E,$$

which is an approximation to the full thermocline feedback from the heat budget, namely $\overline{w} \langle \partial T / \partial z \rangle_E$. The thermocline feedback accounts for the effect of wind stress forcing on the slope of the thermocline, which in turn generates subsurface and surface temperature anomalies. The BJ index approximates $\langle \partial T / \partial z \rangle_E$ in the thermocline feedback by $\langle T_H / H_{BJ} \rangle_E$. Following this, there are three more approximations made in stepping from the heat budget to the BJ index formulation of the thermocline feedback in Jin et al. (2006).

The first coefficient in the thermocline feedback, a_h, can be estimated via regression of the subsurface temperature anomaly $\langle T_H \rangle_E$ against the central-eastern averaged thermocline depth anomaly $\langle h \rangle_E$:

$$\langle H(\overline{w}) T_H \rangle_E = a_h \langle h \rangle_E. \tag{9}$$

This relation was defined only for the scenario when $\overline{w} > 0$. The term $H(\overline{w})$ is the Heaviside step function that ensures only vertical motion into the mixed layer affects the mixed layer temperature. The scatter plot and timeseries of this relation are illustrated in Fig. 3a. In ACCESS-OM, the corresponding regression slope is 2.0 ± 0.1, and the correlation coefficient between $\langle H(\overline{w}) T_H \rangle_E$ and $\langle h \rangle_E$ is 0.91 (Table 1), which indicates that the explained variance is 83 %. This estimate for a_h is consistent with Kim and Jin (2010a).

Secondly, the coefficient β_h can be estimated via regression of the difference in thermocline slope across the equatorial Pacific against the wind stress forcing, namely

$$\langle h \rangle_E - \langle h \rangle_W = \beta_h [\tau^x]. \tag{10}$$

Figure 3b shows the scatter plot and timeseries of this relationship, yielding a β_h value of $16 \times 10 \pm 11$ °C Pa^{-1}, again consistent with the estimate of Kim and Jin (2010a). The variable $[\tau^x]$ explains 74 % of the variance in the thermocline slope.

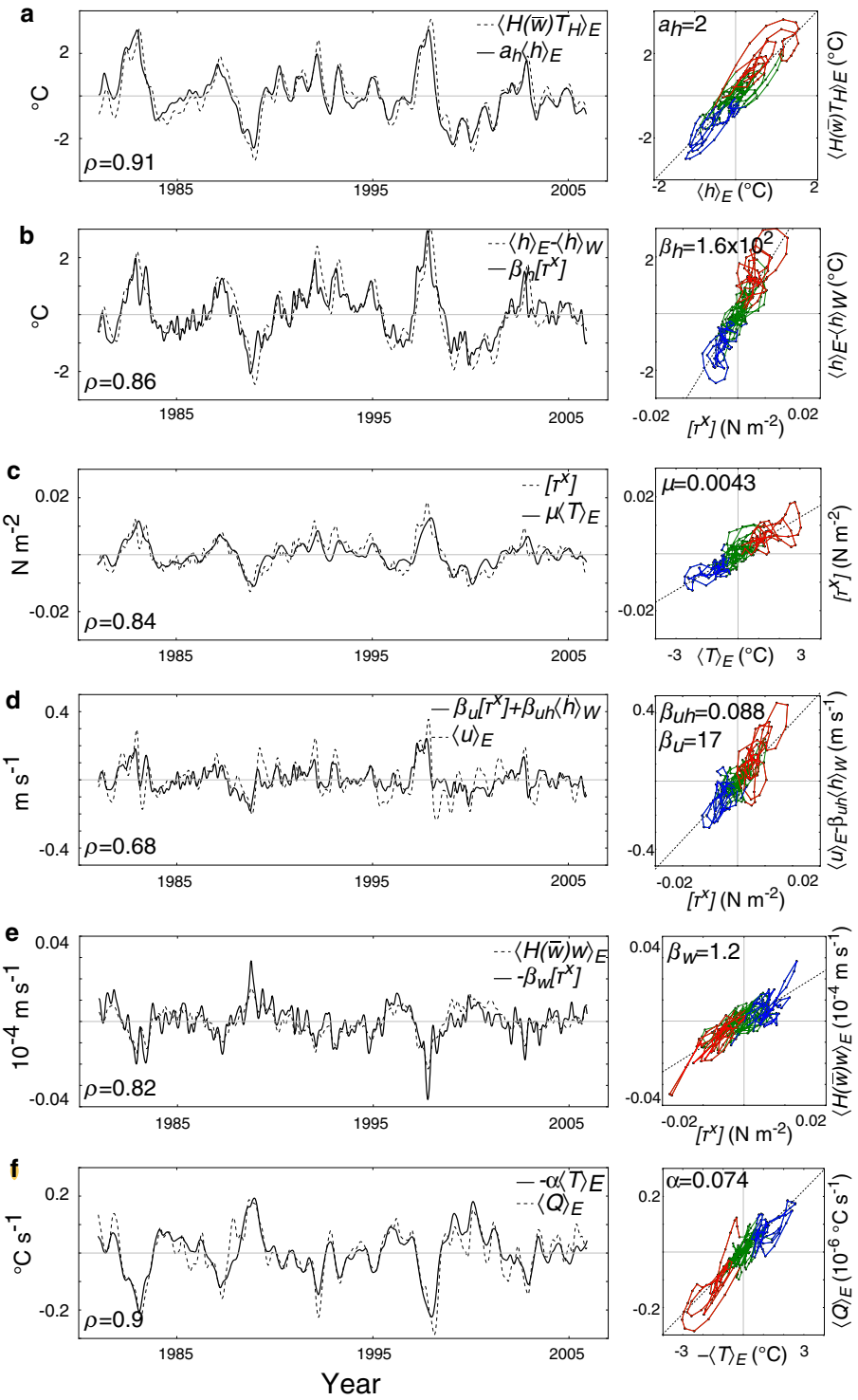

Fig. 3 Timeseries and scatter plots from the balance equations used to derive the BJ index. The scatter plots are colored by El Niño years (*red dots*), La Niña years (*blue dots*), and neutral years (*green dots*). The correlation coefficients between the two timeseries (post-fitting) in *each panel* are reported (ρ values). **a** The *left panel* shows the timeseries of $a_h\langle h\rangle_E$ (*solid line*) and $\langle H(\overline{w})T_H\rangle_E$ (*dashed line*) and the *right panel* shows the scatter plot of these two same variables where the *black dotted slope line* represents the value of the coefficient a_h as estimated from least squares regression of the balance relation $\langle H(\overline{w})T_H\rangle_E = a_h\langle h\rangle_E$, Eq. (9). **b** As in panel **a** except for the balance relation in Eq. (11). Here, the *solid line* in the *left panel* is $\beta_h[\tau^x]$ and the *dashed line* is $\langle h\rangle_E - \langle h\rangle_W$. **c** As in panel **a** except for the balance relation in Eq. (11). Here, the *solid line* in the *left panel* is $\mu\langle T\rangle_E$ and the *dashed line* is $[\tau^x]$. **d** As in panel **a** except for the balance relation in Eq. (13). Here, the *solid line* in the *left panel* is $\beta_u[\tau^x] + \beta_{uh}\langle h\rangle_W$ and the *dashed line* is $\langle u\rangle_E$. **e** As in panel **a** except for the balance relation in Eq. (15). Here, the *solid line* in the *left panel* is $-\beta_w[\tau^x]$ and the *dashed line* is $\langle H(\overline{w})w\rangle_E$. **f** As in panel **a** except for the balance relation in Eq. (17). Here, the *solid line* in the *left panel* is $-\alpha\langle T\rangle_E$ and the *dashed line* is $\langle Q\rangle_E$

Finally, the coefficient representing the sensitivity of the wind response to temperature forcing μ, a component of each of the oceanic feedback terms, can be estimated via regression of the zonal wind stress anomalies onto the temperature anomalies, that is

$$[\tau^x] = \mu\langle T\rangle_E. \tag{11}$$

The scatter plot and timeseries of this relation are shown in Fig. 3c. The regression slope is $0.43 \pm 0.03 \times 10^{-2}$ Pa °C^{-1} and the correlation coefficient between $[\tau^x]$ and $\langle T\rangle_E$ is 0.84. This estimate for μ agrees with those from similar studies (Kim and Jin 2010a; Lübbecke and McPhaden 2013).

Previous studies (e.g. Frauen and Dommenget 2010; Choi et al. 2013) have argued that on ENSO-like timescales there is a nonlinear relationship, rather than a linear one, between zonal wind stress and SST, which gives rise to an asymmetry between El Niño and La Niña events. We find that for the ACCESS-OM run, and using the basin-wide averaged zonal mean wind stress $[\tau^x]$ and central-eastern volume-averaged temperature $\langle T \rangle_E$, there is an approximately 33 % difference in slope between warm events and cool events for the relation in Eq. (11), which indicates that the assumption of linearity is not sufficient. This value for the difference in slope is higher than observed, but is less than the value estimated from the GFDL coupled ocean/atmosphere/land/sea ice model CM2.1 (Choi et al. 2013). However, it should be noted that our value is not directly comparable with the values estimated in Choi et al. (2013) for two primary reasons: (1) we regress the basin-wide average of $[\tau^x]$ with the volume-averaged temperature, rather than the Niño-4 averaged zonal wind stress with the Niño-3.4 averaged SST; and (2) the model data used in this study is an ocean-only run forced by $[\tau^x]$, not a coupled run.

Combining Eqs. (9−11), the BJ index thermocline feedback approximation of the heat budget thermocline feedback is:

$$\langle H(\overline{w})\overline{w}\rangle_E \left\langle \frac{\partial T}{\partial z} \right\rangle_E = a_h \beta_h \mu \left\langle \frac{\overline{w}}{H_{BJ}} \right\rangle_E \langle T \rangle_E + a_h \left\langle \frac{\overline{w}}{H_{BJ}} \right\rangle_E \langle h \rangle_W, \quad (12)$$

where the coefficient that is multiplied by $\langle T \rangle_E$ on the right-hand side of Eq. (12) is the BJ index thermocline feedback that contributes to the growth of an ENSO event R in Eq. (1), and the coefficient that is multiplied by $\langle h \rangle_W$ is a component of the frequency term F in Eq. (1).

The total BJ index thermocline feedback, term (3) in Eq. (7), is 2.9 [− 0.5, + 0.6] year^{-1}, which is larger than the values estimated by Kim and Jin (2010a) and Lübbecke and McPhaden (2013). The larger thermocline feedback in our case is likely due to a larger value of $\langle \overline{w} \rangle_E$ obtained here than in previous studies; however, this is to be expected due to physical and dynamical differences in the models used. For example, the term a_h is sensitive to the model data used and contributes to uncertainty in the value of the thermocline feedback since (1) a_h is a function of the mean ocean stratification, which varies considerably from model to model (e.g. Yeh et al. 2010; Lengaigne et al. 2011); and (2) a_h cannot be fully determined by simple linear regression between $\langle h \rangle_E$ and $\langle T_H \rangle_E$ since the strength of the thermocline feedback depends on the balance between the contributions of zonal and vertical advection to the temperature anomaly tendency (Dewitte et al. 2013).

When multiplied by $\langle T \rangle_E$, as in the first term on the right-hand side of Eq. (12), the thermocline feedback can be compared with the heat budget thermocline feedback, term (3) in Eq. (6) (Fig. 4a). The correlation coefficient between the two curves is 0.60. The BJ index thermocline feedback overestimates the heat budget thermocline feedback due to two key reasons. Firstly, the magnitude of the BJ index thermocline feedback is determined by the magnitude of the coefficient $a_h \beta_h \mu \langle \overline{w}/H_{BJ} \rangle_E$, which multiplies the $\langle T \rangle_E$ term in Eq. (12). It is possible that this coefficient is too large, due to an overestimation of the regression coefficients in Eqs. (9–11), or an overestimation of the mean upwelling $\langle \overline{w} \rangle_E$. Secondly, the BJ index thermocline feedback captures the main features of the low-frequency variability of the heat budget thermocline feedback, which means it may miss some ENSO events when multiple events of the same sign occur in succession. It follows that there are points in time where the BJ index thermocline feedback is large and positive or large and negative, although the heat budget thermocline feedback is near zero.

In order to make a complete comparison of the BJ index thermocline feedback with that of the heat budget, it is necessary to include the components of the thermocline feedback contributing to both growth and frequency, that is, both terms on the right-hand side of Eq. (12). These components are combined and plotted against the heat budget thermocline feedback in Fig. 4b. Although the magnitude of the combined BJ index thermocline feedback is more similar to the heat budget thermocline feedback than the component contributing to growth alone, the correlation between the two timeseries is slightly smaller ($\rho = 0.51$). The biggest discrepancies between the combined BJ index thermocline feedback and the heat budget thermocline feedback occur during central Pacific ENSO events (e.g. 1992–1995 and 1999–2003), which have a less robust recharge mechanism than eastern Pacific events.

3.3 Zonal advective feedback

The zonal advective feedback contribution to the BJ index is

$$\beta_u \mu \left\langle -\frac{\partial \overline{T}}{\partial x} \right\rangle_E,$$

which represents the change in the mixed layer temperature tendency due to the action of anomalous zonal currents on the mean zonal temperature gradient, namely the term $\langle u \rangle_E \langle -\partial \overline{T}/\partial x \rangle_E$ in the heat budget.

The term β_u can be estimated via multiple linear regression from an equation relating the anomalous zonal currents $\langle u \rangle_E$ to forcing by the local anomalous zonal wind

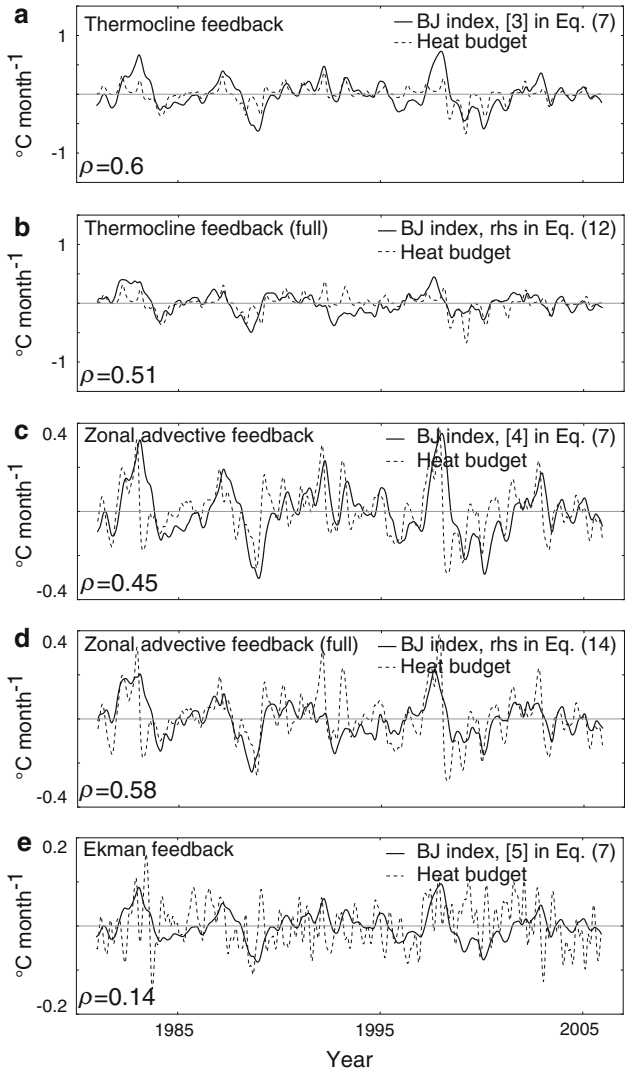

Fig. 4 Oceanic feedbacks from the BJ index (*solid lines*) and their corresponding representation in the heat budget (*dashed lines*). The *panels* show: **a** the thermocline feedback contributing to growth in the BJ index, that is term (3) in Eq. (7); **b** the full thermocline feedback, including both growth and frequency contributions from Eq. (12); **c** the zonal advective feedback contributing to growth in the BJ index, that is term (4) in Eq. (7); **d** the full zonal advective feedback, including both growth and frequency contributions from Eq. (14); and **e** the Ekman feedback contributing to growth in the BJ index, that is term (5) in Eq. (7). Note the different scales on the *y*-axes

stress $[\tau^x]$ and the geostrophic adjustment to the thermocline depth gradient $\langle h \rangle_W$, given by (Jin 1997b)

$$\langle u \rangle_E = \beta_u [\tau^x] + \beta_{uh} \langle h \rangle_W. \tag{13}$$

In the ACCESS-OM run, β_u is 17 ± 2 m s^{-1} Pa^{-1} and β_{uh} is 0.088 ± 0.02 m s^{-1} °C^{-1}. The value for β_u is higher than the value estimated by Lübbecke and McPhaden (2013) for the equatorial Atlantic ocean, although our estimate of β_{uh} is comparable. The scatter plot and timeseries of the relation in Eq. (13), including both the wind stress forcing and the geostrophic adjustment, are illustrated in Fig. 3d. The correlation coefficient is 0.68 and the explained variance is 47 %, both of which are relatively low. Lübbecke and McPhaden (2013) found that this relation was also poor in the observational datasets, although they argued that this is related to the short time period of overlapping years and the poor quality of the thermocline data. However, when a 12-month filter is applied to the variables $\langle u \rangle_E$, $[\tau^x]$, and $\langle h \rangle_W$, the correlation coefficient between the left- and right-hand sides of Eq. (13) increases to 0.81. We note that the basin-wind average of $[\tau^x]$ may not be as appropriate for accurately estimating the sensitivity of the zonal currents to wind forcing as an average of zonal wind stress in the Niño-4 region, where $\langle \partial T / \partial x \rangle_E$ is strong.

Equations (11) and (13) are combined to yield the BJ index zonal advective feedback approximation to the heat budget zonal advective feedback, namely

$$\langle u \rangle_E \left\langle -\frac{\partial \overline{T}}{\partial x} \right\rangle_E = \beta_u \mu \left\langle -\frac{\partial \overline{T}}{\partial x} \right\rangle_E \langle T \rangle_E + \beta_{uh} \left\langle -\frac{\partial \overline{T}}{\partial x} \right\rangle_E \langle h \rangle_W, \tag{14}$$

where the coefficient that is multiplied by $\langle T \rangle_E$ on the right-hand side of Eq. (14) is the BJ index zonal advective feedback and the coefficient that is multiplied by $\langle h \rangle_W$ contributes to the frequency term in Eq. (1).

The zonal advective feedback from the BJ index is 1.4 ± 0.3 year^{-1}, which is greater than previous estimates (c.f. Lübbecke and McPhaden 2013). The zonal advective feedback from the BJ index can be multiplied by $\langle T \rangle_E$, as in Eq. (14), and compared with the corresponding zonal advective feedback from the heat budget (Fig. 4c). The correlation coefficient between the two curves is 0.45, with the BJ index zonal advective feedback explaining 20 % of the variance in the original heat budget zonal advective feedback.

When geostrophic effects are added to the zonal advective feedback from the BJ index, that is, the second term in Eq. (14), the correlation with the heat budget zonal advective feedback increases to 0.58; however, this modified zonal advective feedback does a poorer job of capturing the magnitude of the heat budget zonal advective feedback (Fig. 4d).

3.4 Ekman feedback

The Ekman feedback term in the BJ index is written

$$\beta_w \mu \left\langle -\frac{\partial \overline{T}}{\partial z} \right\rangle_E,$$

and describes the effect on the equatorial temperature tendency of the anomalous wind forced upwelling acting on the mean vertical temperature gradient. It is derived from the term $\langle H(\overline{w}) w \rangle_E \langle \partial \overline{T} / \partial z \rangle_E$.

The coefficient β_w can be estimated by regressing the anomalous upwelling $\langle H(\overline{w})w\rangle_E$ onto the zonal wind stress anomalies $[\tau^x]$, i.e.

$$\langle H(\overline{w})w\rangle_E = -\beta_w[\tau^x], \tag{15}$$

yielding a value of β_w equal to $1.2 \pm 0.09 \times 10^{-4}$ m s^{-1} Pa^{-1}, which is again consistent with the value estimated by Kim and Jin (2010a). The scatter plot and timeseries are shown in Fig. 3e. The correlation coefficient is 0.82, and the explained variance is 68 %. As above for the estimation of β_u, an average of the zonal wind stress anomalies in a region where $\langle \partial T/\partial z\rangle_E$ is strong, rather than over the full equatorial Pacific, may be more appropriate for estimating the sensitivity of $\langle H(\overline{w})w\rangle_E$ to wind forcing.

The BJ index approximation to the heat budget Ekman feedback is found by combining Eqs. (11) and (15), yielding

$$\langle H(\overline{w})w\rangle_E \left\langle \frac{\partial \overline{T}}{\partial z}\right\rangle_E = \beta_w \mu \left\langle -\frac{\partial \overline{T}}{\partial z}\right\rangle_E \langle T\rangle_E. \tag{16}$$

Again, taking into account μ from Sect. 3.2 above, the value of the BJ index Ekman feedback coefficient is 0.38 ± 0.06 year^{-1}. When multiplied by $\langle T\rangle_E$, the BJ index Ekman feedback can be compared with the Ekman feedback from the heat budget (Fig. 4e). The correlation coefficient between the two curves is 0.14. In particular, we note that the BJ index Ekman feedback underestimates the magnitude of the large ENSO events.

3.5 Evaluating the MLD

One difference between the BJ index feedbacks and the corresponding heat budget feedbacks is their definition of MLD. That is, while the BJ index terms are volume averaged in the top 50m of the equatorial Pacific, the heat budget terms are volume averaged between the surface and a variable MLD.

To investigate the difference in magnitudes of the ocean feedbacks that the definition of MLD introduces, we calculate each of the three ocean feedbacks in the mixed layer heat budget equation—the thermocline feedback, the zonal advective feedback and the Ekman feedback—for the case when the MLD varies and for the case when it is held fixed at 50 m depth (Fig. 5). We find that the largest difference between the two MLD definitions arises for the thermocline feedback, where the error is of a similar order of magnitude as the feedback itself. By contrast, there is a smaller difference between the MLD definitions for the zonal advective feedback.

Closer examination of the terms in the BJ index highlights the differences between the cases when the MLD is fixed and when it varies. Central-eastern averaged temperature $\langle T\rangle_E$, and its horizontal derivatives, as well as the zonal current $\langle u\rangle_E$ do not change significantly when averaged in a variable rather than fixed volume. There is a greater difference between the vertical and entrainment velocities, $\langle w\rangle_E$ and $\langle w_e\rangle_E$, respectively, since the latter takes into account horizontal flow at the base of the mixed layer as well as the tendency of the MLD. However, the largest difference arising from the change in MLD definitions is in the term $\langle \partial T/\partial z\rangle_E$, which in the BJ index is parameterized as $\langle T_H/H_{BJ}\rangle_E$. When the MLD is allowed to vary, the variance in $\langle T_H/H_{BJ}\rangle_E$ increases markedly due to the large change in H_{BJ}. It is for this reason that the thermocline and Ekman feedbacks are so noticeably different for the two MLD definitions.

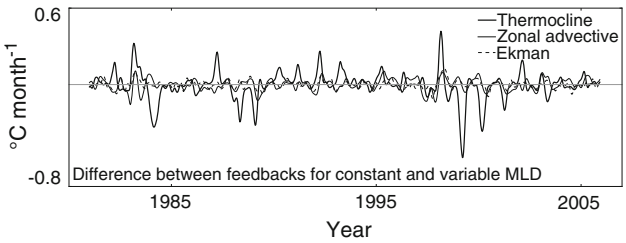

Fig. 5 Difference between the cases when the MLD is variable and fixed at 50m for: the heat budget thermocline feedback (*dark solid line*), the zonal advective feedback (*light solid line*), and the Ekman feedback (*dashed line*)

3.6 Other BJ index terms

In the previous sections we contrast the BJ index ocean feedbacks with the corresponding terms from the heat budget. In what follows we calculate the BJ index terms that quantify thermodynamic damping and advection by mean currents.

3.6.1 Thermodynamic damping

The thermodynamic damping coefficient, denoted α, is calculated via linear regression of the local net downward surface heat flux anomalies onto the volume averaged temperature anomalies in the central-eastern equatorial box, namely

$$\langle Q\rangle_E = -\alpha\langle T\rangle_E. \tag{17}$$

Here, $\langle Q\rangle_E$ is scaled by the constants $\rho = 1035$ kg m^{-3} and $c_p = 3989.24$ J kg^{-1} °C^{-1} to be of the same units as $\alpha\langle T\rangle_E$. The value of α is 2.3 ± 0.1 year^{-1} in our model run, and the scatter plot and timeseries are shown in Fig. 3f. This value is slightly higher than values reported in previous studies (e.g. Kim and Jin (2010a) and Lübbecke and McPhaden (2013) estimate α to be between 1.30 and

1.90 year^{-1}), but generally within the 95 % CIs of these previous estimates. The correlation coefficient between $\langle Q \rangle_E$ and $\langle T \rangle_E$ is 0.90. As the accuracy of the BJ index formulation of the thermodynamic damping term from the heat budget equation has already been studied (e.g. Lloyd et al. 2012), we do not compare it with the corresponding term from the heat budget here.

Surface heat fluxes are the largest contributor to damping in the central equatorial Pacific, and are dominated by the shortwave (Q_{SW}) and latent heat fluxes (Lloyd et al. 2011). Previous studies (e.g. Lloyd et al. 2012; Bellenger et al. 2013) argue that the cloud processes described in the shortwave feedback (i.e. the coefficient α_{SW} estimated via regression of the shortwave heat flux $\langle Q_{SW} \rangle_E$ with $\langle T \rangle_E$) are highly complex, implying that the linear relationship between $\langle Q \rangle_E$ and $\langle T \rangle_E$ described above is perhaps over simplified. Hence, it is likely that the uncertainty associated with our value of α is larger than estimated above. However, given that our focus in this study is on the representation of the ocean feedbacks important to ENSO, we do not investigate this matter further.

3.6.2 Advection by mean currents

The remaining terms in Eq. (22) from the "Appendix" represent advection of the temperature averaged in the central-eastern equatorial box due to mean zonal, meridional, and vertical currents, namely

$$-\left(\frac{\langle \overline{u} \rangle_E}{L_x} + \frac{\langle -2y\overline{v} \rangle_E}{L_y^2} + \frac{\langle \overline{w} \rangle_E}{H_{BJ}}\right), \tag{18}$$

which are collectively -1.9 year^{-1}.

3.7 Total BJ index

The terms in Eq. (7), as estimated in Sects. 3.2–3.6, are summed, yielding a BJ index of 0.49 [$-$ 0.2, $+$ 1] year^{-1}, illustrated in Fig. 6. The largest contributor to the instability growth is the thermocline feedback, and the largest damping is from mean advection. The BJ index, R, is negative and as it sets the growth of the recharge oscillator model from Eq. (1), it is clear that the system is unstable in the ACCESS-OM simulation for the period 1980-2007. The largest uncertainty associated with the estimate of R for our model comes from the ocean feedbacks, and in particular the thermocline and zonal advective feedbacks, respectively. The error estimate associated with the total BJ index is very large, due to the cumulative uncertainties associated with the estimates of the regression coefficients. It is unlikely that the error estimate associated with the BJ index would improve if a longer, coupled model run were to be employed due to the range of ENSO behaviors in CGCMs.

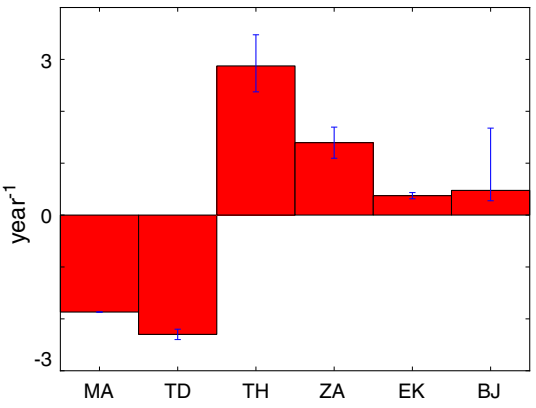

Fig. 6 The BJ index and its contributing terms. MA represents advection by mean currents, *TD* is thermodynamic damping, *TH* is the thermocline feedback, *ZA* is the zonal advective feedback, *EK* is the Ekman feedback, and *BJ* is the BJ index, *R*

4 Discussion

The BJ index quantifies the positive feedback (instability growth) in the recharge oscillator model, and is used to understand the stability properties of ENSO as described by that model. The BJ index is derived from a series of balance equations and approximations to the mixed layer heat budget equation. We have explored the robustness of these approximations and their implications for the representations of the ocean feedbacks important to ENSO in the BJ index. We found that the approximations did not always accurately portray the ocean dynamics they described and could be misleading for model intercomparisons.

One of the largest inconsistencies between the heat budget feedbacks and the corresponding BJ index parameterization arose due to an overestimation of the correlation between each. For example, noting that the correlation coefficient is the cosine of the angle between two vectors, suppose that the vectors A and B are orthogonal so that $\rho_{AB} = 0$. Now, suppose vector C bisects the right angle between A and B. Then $\rho_{AC} = \rho_{BC} = \cos(\pi/4) \approx 0.7$, such that A and B account for approximately 50 % of the variance in C, despite having no variance in common. In the case of the Ekman feedback, the individual balance relations used to derive the BJ index feedback from that of the heat budget were highly correlated: the timeseries of wind stress anomalies $[\tau^x]$ and temperature anomalies $\langle T \rangle_E$ from Eq. (11) had a correlation coefficient of 0.84, and the timeseries of vertical velocity anomalies $\langle H(\overline{w})w \rangle_E$ and wind stress anomalies $[\tau^x]$ had a correlation coefficient of 0.82. However, the correlation coefficient between the original heat budget Ekman feedback and the BJ index Ekman feedback was only 0.14.

A second source of error in the BJ index formulation was the assumption of linearity in the balance relations Eqs. (9–11), (13), (15), and (17). It is well known that the wind stress feedback is a nonlinear function of SST (Wang and McPhaden 2000; Jin et al. 2003; Timmermann et al. 2003; An and Jin 2004; Gebbie et al. 2007; Brown et al. 2010) and this is highlighted by the balance relation in Eq. (13) where the linear approximation could only explain 47 % of the variance in the zonal current anomaly. Although nonlinearities were not explicitly included in the BJ index, large ENSO events, or those events with markedly different dynamics, had an influence on the determination of the regression coefficients in the BJ index calculation. Furthermore, given the range of ENSO behaviors within a GCM with constant external forcing (Wittenberg, 2009; Kug et al. 2010; Ogata et al. 2013), it is possible that there will be periods in the future marked by different flavors of ENSO where the nonlinear terms will be more important (Vecchi et al. 2006).

A third problem that has been identified from our analysis relates to the use of regression coefficients in constructing the BJ index feedbacks. Regression coefficients do not tell us whether each of the timeseries used in the analysis are lagged, nor do they provide information on the similarities and differences between the curves. We illustrate this point with the use of a theoretical model in Fig. 7. We calculate a regression coefficient between time series R (red curve) and each of A—a timeseries of the same magnitude and shape as R, but lagged by $\pi/3$ units—and B—a timeseries with a magnitude up to 1.75 times that of R and with a different shape. Both calculations result in a regression coefficient of 0.5, suggesting that the sensitivity between R and A is the same as R and B. If we apply a similar argument to the BJ index, we conclude that the magnitude of the BJ index feedbacks may be over- or underestimated, which is clear from comparison of the BJ index thermocline feedback with the heat budget feedback in Fig. 4a. That the BJ index may over- or underestimate feedback magnitudes has implications for the usefulness of model intercomparisons.

A fourth difference between the BJ index feedbacks and the heat budget feedbacks was due to the different parameterizations of the MLD. While the heat budget ocean feedbacks were calculated within a temporally and spatially varying MLD, the BJ index assumed that the MLD was a constant 50m. Although 50m is close to the mean MLD across the equatorial Pacific, it is nevertheless a gross approximation to the true MLD and does not provide a realistic expression of the oceanic processes that give rise to mixed layer temperature variations. For example, a constant mixed layer depth will not capture the changes in stratification associated with a deepening thermocline during El Niño events (DiNezio et al. 2012). Given that a robust estimate of the MLD is a standard output in most models, it is not costly to include the more accurate representation of ocean dynamics via a varying MLD rather than a fixed MLD in calculating the BJ index feedback terms.

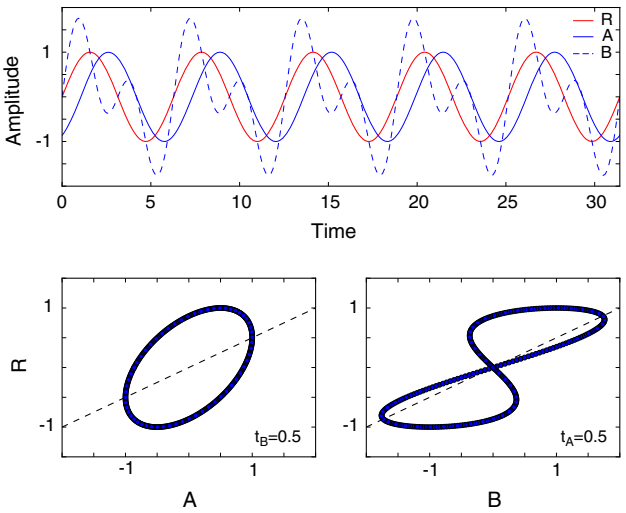

Fig. 7 Toy model highlighting the problem with using the regression coefficient as an estimate of the similarity between feedbacks. The *top panel* shows the timeseries of R (*red line*), A (*blue solid line*), and B (*blue dashed line*). The *lower left panel* shows the regression between R and A; the *lower right panel* shows the regression between the R and B. Note that the regression coefficients, t_A and t_B, for the regressions in the *lower panels* are equal

Finally, the values of the feedbacks estimated by the BJ index will depend on the time period and region over which they are calculated. We estimated the averaging domain by EOF analysis of 28 years of heat content anomaly data, but even within this period there were different spatial "flavors" of ENSO (e.g. both canonical eastern Pacific events and central Pacific events as in Ashok et al. 2007) such that the BJ index results may be inadvertently weighted towards a particular spatial signal of ENSO.

5 Summary

In the original paper on the BJ index, Jin et al. (2006) used an intermediate complexity model to demonstrate that the BJ index is a good approximation to the coupled slow instability of ENSO. As a result, they argued that the BJ index can be used instead of eigenanalysis, which is not feasible in many CGCMs, to assess how the leading, linear ENSO-like mode might change under different background states of the equatorial Pacific. Since then, the BJ index has been widely used in model intercomparisons of complex,

nonlinear CGCMs with variable MLDs to assess changes in ENSO feedbacks from historical periods to periods with increased CO_2 forcing (e.g. Kim and Jin 2010a; Bellenger et al. 2013). We argue that since the BJ index misrepresents the true magnitude of the ENSO ocean feedbacks—namely the thermocline, zonal advective, and Ekman feedbacks—as calculated using the mixed layer heat budget equation for the tropical ocean, it should be used with caution as a diagnostic tool to assess model behavior and biases. Furthermore, when assessing dynamical differences between models it may be more fruitful to calculate the heat budget feedbacks directly, which explicitly account for nonlinearities that are not parameterized in the BJ index.

Our analysis was restricted to an ocean-only GCM run over a short period; however, we argue that the use of a flux-forced ocean/sea ice model (that is comparable to observational products) is preferable in this instance to a coupled ocean/atmosphere/sea ice model, which may suffer biases that can complicate the representation of ocean–atmosphere interactions in the tropical Pacific. The ACCESS-OM simulation has been useful in understanding the workings of the BJ index formula and its shortcomings. We are hopeful that the BJ index can be improved by incorporating appropriate nonlinearities into the balance relations that underlie each of the feedbacks and by including a temporally and spatially varying MLD. However, this may be challenging given the uncertainties associated with future changes in ENSO behavior, limited observational data, and differing ENSO behavior across models.

Based on the recharge discharge oscillator model, the BJ index is a powerful tool for diagnosing the stability of the leading ENSO-like mode in coupled models; however, we have demonstrated that the BJ index does not adequately describe the dynamics of the ocean feedbacks of ENSO. As a consequence, its application in the assessment of model behavior, biases, and intercomparisons, particularly under climate change scenarios, should be conducted with caution, being fully mindful of the pitfalls and limitations described here.

Acknowledgments We would like to thank Dietmar Dommenget and Simon Wotherspoon for helpful discussions on this work, and SeonTae Kim, Agus Santoso and two anonymous reviewers for providing useful feedback to improve the manuscript. The ACCESS-OM model is supported by the Australian Government Department of the Environment, the Bureau of Meteorology and CSIRO through the Australian Climate Change Science Program, and the NCI National Facility at the ANU. The CARS MLD product was derived from the CSIRO Atlas of Regional Seas from CSIRO Marine and Atmospheric Research. This research is supported by an Australian Postgraduate Award and a CSIRO Wealth from Oceans scholarship and makes a contribution to the ARC Centre of Excellence for Climate System Science.

Appendix

Derivation of the BJ index

The BJ index is derived from the linearized anomalous temperature tendency equation, namely

$$\frac{\partial T'}{\partial t} = -\overline{u}\frac{\partial T'}{\partial x} - \overline{v}\frac{\partial T'}{\partial y} - \overline{w}\frac{\partial T'}{\partial z} - u'\frac{\partial \overline{T}}{\partial x} - v'\frac{\partial \overline{T}}{\partial y} - w'\frac{\partial \overline{T}}{\partial z} + Q'_q, \tag{19}$$

where the overline notation denotes climatological fields (i.e. averaged over the full time period) and the prime denotes anomalous fields that have the seasonal cycle removed. In what follows we drop the prime notation. The terms in Eq. (19) are averaged vertically, from the ocean surface to the MLD, and horizontally in the central-eastern equatorial Pacific 5°S–5°N, 175°E–80°W), in which the majority of ENSO variability occurs, yielding

$$\left\langle \frac{\partial T}{\partial t} \right\rangle_E = -\left(\frac{\langle \overline{u} \rangle_E}{L_x} + \frac{\langle -2y\overline{v} \rangle_E}{L_y^2} + \frac{\langle \overline{w} \rangle_E}{H_{BJ}} \right) \langle T \rangle_E + \langle Q \rangle_E - \left\langle \frac{\partial \overline{T}}{\partial x} \right\rangle_E \langle u \rangle_E - \left\langle \frac{\partial \overline{T}}{\partial z} \right\rangle_E \langle H(\overline{w}) w \rangle_E + \left\langle \frac{\overline{w}}{H_{BJ}} \right\rangle_E \langle H(\overline{w}) T_H \rangle_E, \tag{20}$$

where L_x and L_y are the longitudinal and latitudinal extents of the central-eastern box, respectively, and the factor $-2y/L_y$ assumes that the tropical SST anomalies are Gaussian with an e-folding decay scale of L_y. The term H_{BJ} is the MLD, T_H is the temperature at the grid point just below the mixed layer, and $H(\overline{w})$ ensures that only the vertical motion into the mixed layer affects the mixed layer heat budget. Note that in deriving Eq. (20), the small term $-v'\partial T/\partial y$ has been omitted, consistent with Jin et al. (2006). A series of balance equations from section 3 [Eqs. (9–11), (13), (15), and (17)] are applied to approximate the terms in Eq. (20). These balance equations yield coefficients that estimate the strength of the air–sea coupling μ, the sensitivity of oceanic responses to surface winds β_h, β_u, β_w, and the magnitude of advection by mean currents and thermodynamic damping. Collectively, they enable the temperature tendency in Eq. (20) to be separated into growth and frequency components, expressed in the form of the recharge oscillator model (Jin 1997a), namely,

$$\left\langle \frac{\partial T}{\partial t} \right\rangle_E = R\langle T \rangle_E + F\langle h \rangle_W. \tag{21}$$

Here the coefficients R and F are explicit functions of the basic state, rather than simply coefficients estimated via

regression to observations or model data. R is the growth term that underpins the BJ index, and is given by

$$R = -\left(\frac{\langle \overline{u} \rangle_E}{L_x} + \frac{\langle -2y\overline{v} \rangle_E}{L_y^2} + \frac{\langle \overline{w} \rangle_E}{H_{BJ}}\right) - \alpha + a_h \beta_h \mu \left\langle \frac{\overline{w}}{H_{BJ}} \right\rangle_E + \beta_u \mu \left\langle -\frac{\partial \overline{T}}{\partial x} \right\rangle_E + \beta_w \mu \left\langle -\frac{\partial \overline{T}}{\partial z} \right\rangle_E, \tag{22}$$

and the frequency term F is given by

$$F = \beta_{uh} \left\langle -\frac{\partial \overline{T}}{\partial x} \right\rangle_E + a_h \left\langle \frac{\overline{w}}{H_{BJ}} \right\rangle_E. \tag{23}$$

References

Adcroft A, Campin JM (2004) Rescaled height coordinates for accurate representation of free-surface flows in Ocean circulation models. Ocean Model 7:269–284

An SI, Jin FF (2001) Collective role of thermocline and zonal advective feedbacks in the ENSO mode. J Clim 14:3421–3432

An SI, Jin FF (2004) Nonlinearity and asymmetry of ENSO. J Clim 17:2399–2412

Ashok K, Behera SK, Rao SA, Weng H, Yamagata T (2007) El Niño Modoki and its possible teleconnection. J Geophys Res 112(C11):1–27. doi:10.1029/2006JC003798

Battisti DS (1988) The dynamics and thermodynamics of a warming event in a coupled tropical atmosphere/Ocean model. J Atmos Sci 45:2889–2919

Battisti DS, Hirst AC (1989) Interannual variability in a tropical atmosphere-Ocean model: influence of the basic State, Ocean geometry and nonlinearity. J Atmos Sci 46(12):1687–1712

Bellenger H, Guilyardi E, Leloup J, Lengaigne M, Vialard J (2013) ENSO representation in climate models: from CMIP3 to CMIP5. Clim Dyn. doi:10.1007/s00382-013-1783-z

Bi D, Marsland SJ, Uotila P, O'Farrell S, Fiedler R, Sullivan A, Griffies SM, Zhou X, Hirst AC (2013) ACCESS-OM: the Ocean and Sea Ice core of the ACCESS coupled model. Aust Meteorol Oceanogr J 63(1):213–232

Bjerknes J (1969) Atmospheric teleconnections from the equatorial Pacific. Mon Weather Rev 97(3):163–172

Brown JN, Godfrey JS, Wijffels SE (2010) Nonlinear effects of tropical instability waves on the equatorial Pacific circulation. J Phys Oceanogr 40(2):381–393. doi:10.1175/2009JPO3963.1

Cane MA, Zebiak SE (1985) A theory for El Nino and the Southern qscillation. Science (New York, NY) 228(4703):1085–7. doi:10.1126/science.228.4703.1085

Choi KY, Vecchi GA, Wittenberg AT (2013) ENSO Transition, duration and amplitude asymmetries: role of the nonlinear wind stress coupling in a conceptual model. J Clim pp 1–36

Collins M, An SI, Cai W, Ganachaud A, Guilyardi E, Jin FF, Jochum M, Lengaigne M, Power S, Timmermann A, Vecchi GA, Wittenberg AT (2010) The impact of global warming on the Tropical Pacific Ocean and El Niño. Nat Geosci 3:391–397

Danabasoglu G, Yeager S, Bailey D, Behrens E, Bentsen M, Bi D, Biastoch A, Boening C, Bozec A, Canuto V, Cassou C, Chassignet E, Coward A, Danilov S, Diansky N, Drange H, Farneti R, Fernandez E, Fogli PG, Forget G, Fujii Y, Griffies S, Gusev A, Heimbach P, Howard A, Jung T, Kelley M, Large W, Leboissetier A, Lu J, Madec G, Marsland S, Masina S, Navarra A, Nurser AG, Pirani A, Salas y Melia D, Samuels B, Scheinert M, Sidorenko D, Treguier AM, Tsujino H, Uotila P, Valcke S, Voldoire A, Wang Q (2014) North Atlantic simulations in coordinated ocean-ice reference experiments phase ii (CORE-II). Part I: Mean states.. Ocean Model 73:76–107. doi:10.1016/j.ocemod.2013.10.005

Dewitte B, Yeh SW, Thual S (2013) Reinterpreting the thermocline feedback in the western-central equatorial Pacific and its relationship with the ENSO modulation. Clim Dyn 41:819–830. doi:10.1007/s00382-012-1504-z

DiNezio PN, Kirtman BP, Clement AC, Lee SK, Vecchi GA, Wittenberg A (2012) Mean climate controls on the simulated response of ENSO to increasing greenhouse gases. J Clim 25(21):7399–7420. doi:10.1175/JCLI-D-11-00494.1

Fedorov AV, Philander SG (2001) A stability analysis of Tropical ocean–atmosphere interactions: bridging measurements and theory for El Nino. J Clim 14(1998):3086–3101

Frauen C, Dommenget D (2010) El Niño and La Niña amplitude asymmetry caused by atmospheric feedbacks. Geophys Res Lett 37(18):L18,801. doi:10.1029/2010GL044444

Gebbie G, Eisenman I, Wittenberg AT, Tziperman E (2007) Modulation of westerly wind bursts by sea surface temperature: a semistochastic feedback for ENSO. J Atmos Sci 64:3281–3295

Griffies SM (2009) Elements of MOM4p1: GFDL Ocean Group Tech. Rep. 6. NOAA/Geophysical Fluid Dynamics Laboratory

Griffies SM, Winton M, Samuels B, Danabasoglu G, Yeager S, Marsland S, Drange H, Bentsen M (2012) Datasets and protocol for the CLIVAR WGOMD coordinated ocean-sea ice reference experiments (COREs). WCRP Report No. 21/2012, pp. 21

Guilyardi E, Wittenberg AT, Fedorov AV, Collins M, Wang C, Capotondi A, van Oldenborgh GJ, Stockdale T (2009) Understanding El Niño in ocean–atmosphere general circulation models: progress and understanding. Bull Am Meteorol Soc March 90:325–340. doi:10.1175/2010JCLI3373.1

Huang B, Xue Y, Zhang D, Kumar A, McPhaden MJ (2010) The NCEP GODAS Ocean analysis of the Tropical Pacific mixed layer heat budget on seasonal to interannual time scales. J Clim 23(18):4901–4925. doi:10.1175/2010JCLI3373.1

Huang B, Xue Y, Wang H, Wang W, Kumar A (2011) Mixed layer heat budget of the El Niño in NCEP climate forecast system. Clim Dyn 39(1-2):365–381. doi:10.1007/s00382-011-1111-4

Hunke E, Lipscomb W (2010) CICE: the Los Alamos Sea Ice Model Documentation and Software User's Manual. Los Alamos, LA-CC-06-012 Tech. Rep. edn

Jin FF (1997) An equatorial ocean recharge paradigm for ENSO. Part I: conceptual model. J Atmos Sci 54:811–829

Jin FF (1997) An equatorial ocean recharge paradigm for ENSO. Part II: A stripped-down coupled model. J Atmos Sci 54:830–847

Jin FF, An SI (1999) Thermocline and zonal advective feedbacks within the equatorial ocean recharge oscillator model for ENSO. Geophys Res Lett 26(19):2989–2992

Jin FF, An SI, Timmermann A, Zhao J (2003) Strong El Niño events and nonlinear dynamical heating. Geophys Res Lett 30(3):1120. doi:10.1029/2002GL016356

Jin FF, Kim ST, Bejarano L (2006) A coupled-stability index for ENSO. Geophys Res Lett 33(23):L23,708. doi:10.1029/2006GL027221

Karnauskas KB (2013) Can we distinguish canonical El Niño from Modoki?. Geophys Res Lett 40:5246–5251. doi:10.1002/grl.51007

Kessler WS, Rothstein LM, Chen D (1998) The annual cycle of SST in the Eastern Tropical Pacific, diagnosed in an ocean GCM. J Clim 11:777–799

Kim ST, Jin FF (2010) An ENSO stability analysis. Part I: results from a hybrid coupled model. Clim Dyn 36(7-8):1593–1607. doi:10.1007/s00382-010-0796-0

Kim ST, Jin FF (2010) An ENSO stability analysis. Part II: results from the twentieth and twenty-first century simulations of the

CMIP3 models. Clim Dyn 36(7-8):1609–1627. doi:10.1007/s00382-010-0872-5
Kim ST, Cai W, Jin FF, Yu JY (2013) ENSO Stability in coupled climate models and its association with mean state. Clim Dyn doi:10.1007/s00382-013-1833-6
Kug JS, Choi J, An SI, Jin FF, Wittenberg A (2010) Warm pool and cold tongue El Niño events as simulated by the GFDL 2.1 coupled GCM. J Clim 23:1226–1239
Large W, Yeager S (2009) The global climatology of an interannually varying air–sea flux data set. Clim Dyn 33: 341. doi:10.1007/s00,382-008-0441-3
Large W, McWilliams J, Doney S (1994) Oceanic vertical mixing: a review and a model with a nonlocal boundary layer parameterization. Rev Geophys 32(4):363–403
Lee HC, Rosati A, Spelman M (2006) Barotropic tidal mixing effects in a coupled climate model: oceanic conditions in the Northern Atlantic. Ocean Model 3(4):464–477
Lengaigne M, Hausmann U, Madec G, Menkes CE, Vialard J, Molines JM (2011) Mechanisms controlling warm water volume interannual variations in the equatorial Pacific: diabatic versus adiabatic processes. Clim Dyn 38(5-6):1031–1046. doi:10.1007/s00382-011-1051-z
Lloyd J, Guilyardi E, Weller H (2011) The role of atmosphere feedbacks during ENSO in the CMIP3 models. Part II: using AMIP runs to understand the heat flux feedback mechanisms. Clim Dyn 37(7-8):1271–1292. doi:10.1007/s00382-010-0895-y
Lloyd J, Guilyardi E, Weller H (2012) The role of atmosphere feedbacks during ENSO in the CMIP3 models. Part III: the shortwave flux feedback. J Clim 25(12):4275–4293. doi:10.1175/JCLI-D-11-00178.1
Lübbecke JF, McPhaden MJ (2013) A comparative stability analysis of Atlantic and Pacific Niño modes. J Clim 26:5965–5980. doi:10.1175/JCLI-D-12-00758.1
Murray R (1996) Explicit generation of orthogonal grids for ocean models. J Comput Phys 126(2):251–275. doi:10.1006/jcph.1996.0136
Neelin JD, Jin FF (1993) Modes of interannual tropical ocean–atmosphere interactions - a unified view. Part II: analytical results in the weak-coupling limit. J Atmos Sci 50(21):3504–3522
Ogata T, Xie SP, Wittenberg AT, Sun DZ (2013) Interdecadal amplitude modulation of El Niño/Southern oscillation and its impacts on Tropical Pacific decadal variability. J Clim. doi:10.1175/JCLI-D-12-00415.1
Oke PR, Sakov P, Cahill ML, Dunn JR, Fiedler R, Griffin DA, Mansbridge JV, Ridgway KR, Schiller A (2013) Towards a dynamically balanced eddy-resolving ocean reanalysis: BRAN3. Ocean Model 67:52–70. doi:10.1016/j.ocemod.2013.03.008
Philander SGH (1990) El Niño, La Niña and the Southern oscillation. Academic Press, Waltham, p 289
Philander SGH, Yamagata T, Pacanowski RC (1984) Unstable air-sea interactions in the tropics. J Atmos Sci 41(4):604–613
Picaut J, Ioualalen M, Menkes C, Delcroix T, McPhaden M (1996) Mechanism of the zonal displacements of the Pacific warm pool: implications for ENSO. Science (New York, NY) 274(5292):1486–9
Qu T (2003) Mixed layer heat balance in the Western North Pacific. J Geophys Res 108(C7):3242. doi:10.1029/2002JC001536
Rebert J, Donguy J, Eldin G (1985) Relations between sea level, thermocline depth, heat content, and dynamic height in the Tropical Pacific Ocean. J Geophys Res 90(C6):11719–11725
Ren H, Jin FF (2013) Recharge oscillator mechanisms in two types of ENSO. J Clim. doi:10.1175/JCLI-D-12-00601.1
Ridgway KR, Dunn JR, Wilkin J (2002) Ocean interpolation by four-dimensional least squares - application to the waters around Australia. J Atmos Ocean Technol 19(9):1357–1375
Santoso A, Sen Gupta A, England MH (2010) Genesis of Indian Ocean mixed layer temperature anomalies: a heat budget analysis. J Clim 23(20):5375–5403. doi:10.1175/2010JCLI3072.1
Schiller A, Ridgway KR (2013) Seasonal mixed layer dynamics in an eddy-resolving Ocean circulation model. J Geophys Res 118:1–19. doi:10.1002/jgrc.20250
Schopf PS, Suarez MJ (1988) Vacillations in a coupled ocean–atmosphere model. J Atmos Sci 45(3):549–566
Sen Gupta A, Brown JR, Muir LC, Risbey JS, Whetton P, Zhang X, Ganachaud A, Murphy B, Wijffels SE (2012) Implications of CMIP3 model biases and uncertainties for climate projections in the western tropical Pacific. Climatic Change. doi:10.1007/s10584-012-0603-5
Simmons H, Jayne S, Laurent L, Weaver A (2004) Tidally driven mixing in a numerical model of the ocean general circulation. Ocean Model 6:245–263
Singh A, Delcroix T, Cravatte S (2011) Contrasting the Flavors of El Niño-Southern Oscillation using Sea Surface Salinity Observations. Journal of Geophysical Research 116(C06016). doi:10.1029/2010JC006862
Smith NR (1995) The BMRC ocean thermal analysis system. Aust Meteorol Mag 44:93–110
Timmermann A, Jin FF, Abshagen J (2003) A nonlinear theory for El Nino bursting. J Atmos Sci 60:152–165
Vecchi GA, Wittenberg AT (2010) El Niño and Our Future Climate: Where do We Stand? Wiley Interdisciplinary Reviews: Climate Change 1(April), doi:10.1002/wcc.33
Vecchi GA, Wittenberg AT, Rosati A (2006) Reassessing the Role of Stochastic Forcing in the 1997-8 El Niño. Geophysical Research Letters L01706. doi:10.1029/2005GL024,738
Wang W, McPhaden MJ (2000) The surface-layer heat balance in the Equatorial Pacific Ocean. Part II: interannual variability. J Phys Oceanogr 30:2989–3008
Watanabe M, Kug JS, Jin FF, Collins M, Ohba M, Wittenberg AT (2012) Uncertainty in the ENSO amplitude change from the past to the future. Geophys Res Lett 39(20):1–6. doi:10.1029/2012GL053305
Wittenberg AT (2009) Are historical records sufficient to constrain ENSO simulations? Geophys Res Lett 36(12):L12,702 doi:10.1029/2009GL038710
Wyrtki K (1975) El Nino - the dynamic response of the Equatorial Pacific Ocean to atmospheric forcing. J Phys Oceanogr 5:572–584
Yeh SW, Dewitte B, Yim BY, Noh Y (2010) Role of the upper ocean structure in the response of ENSO-like SST variability to global warming. Clim Dyn 35:355–369. doi:10.1007/s00382-010-0849-4
Zebiak SE, Cane MA (1987) A model El Nino-Southern oscillation. Mon Weather Rev 115:2262–2278
Zhang X, McPhaden MJ (2010) Surface layer heat balance in the Eastern Equatorial Pacific Ocean on interannual time scales: influence of local versus remote wind forcing. J Clim 23(16):4375–4394. doi:10.1175/2010JCLI3469.1